Isı Bilimi ve Tekniği Dergisi, 37, 2, 19-32, 2017
J. of Thermal Science and Technology

ISSN 1300-3615

EFFECTS OF FLOW ROUTING PLATE ON MIXED CONVECTION HEAT TRANSFER FROM PROTRUDED HEAT SOURCES

Burak KURŞUN* and Mecit SİVRİOĞLU**
*Amasya Üniversitesi Teknoloji Fakültesi Makina Mühendisliği Bölümü
Merkez, Amasya, burak.kursun@amasya.edu.tr
** Gazi Üniversitesi Mühendislik Fakültesi Makina Mühendisliği Bölümü
06570 Maltepe, Ankara, mecits@gazi.edu.tr

(Geliş Tarihi: 20.09.2016, Kabul Tarihi: 02.01.2017)

Abstract: In this study, the effect of the flow routing plates on the laminar mixed convection heat transfer in a horizontal channel that has protruded heat sources at the bottom and top surfaces were investigated numerically and experimentally. The air was used as the cooling fluid, and protruded heat sources were equipped as 4x8 rows into the rectangle channel that has insulated walls. The experimental study was applied for two different Reynolds (Re) numbers. A numerical model complying with the experimental results was created, and numerical investigations were performed in different Reynolds and modified Grashof (Gr*) numbers for the 0°, 30°, 60° values of the plate angles (α). The analyses showed that using flow routing plate only increases the heat transfer from the first four heater rows on the bottom surface, and the first and the last heater rows on the top surface. The findings obtained during the experimental and numerical studies were presented in detail as graphics showing the row averaged Nusselt number ($Nu_{row\ ave.}$), the heater temperatures, velocity vectors, and temperature contours.
Keywords: Flow routing plate, Horizontal channel, Mixed convection, Protruded heat sources

AKIŞ YÖNLENDİRİCİ PLAKANIN ÇIKINTILI ISI KAYNAKLARINDAN KARIŞIK KONVEKSİYONLA ISI TRANSERİNE ETKİSİ

Özet: Bu çalışmada, akış yönlendirici plaka kullanımının alt ve üst yüzeylerinde çıkıntılı ısı kaynakları bulunan yatay bir kanal içerisindeki karışık konveksiyonla laminar ısı transferine etkisi sayısal ve deneysel olarak incelenmiştir. Soğutucu akışkan olarak hava kullanılmış olup ısı kaynakları duvarları yalıtılmış olan dikdörtgen kanal içerisine 8x4'lük diziler halinde yerleştirilmiştir. Deneysel çalışma iki farklı Reynolds sayısı (Re) için yapılmıştır. Deneysel çalışma sonuçları ile uyumlu bir sayısal model oluşturulmuş ve sayısal çalışma 0°, 30°, 60° plaka açıları için farklı Re ve Grashof (Gr) sayılarında gerçekleştirilmiştir. Analizler akış yönlendirici plaka kullanımının yalnızca alt yüzeyde ilk dört ısıtıcı sırası için, üst yüzeyde ise ilk ve son ısıtıcı sıraları için ısı transferini artırdığını göstermiştir. Deneysel ve sayısal çalışma sırasında elde edilen bulgular sıra ortalama Nusselt sayısı ($Nu_{sıra\ ort.}$), ısıtıcı sıcaklıkları, hız vektörleri ve sıcaklık kontörlerini gösteren grafikler halinde ayrıntılı olarak sunulmuştur.
Anahtar Kelimler: Akış yönledirici plaka, Yatay kanal, Karışık konveksiyon, Çıkıntılı ısı kaynakları

NOMENCLATURE

A	heat transfer area, [m^2]
A_k	channel cross-sectional area, [m^2]
A_{heater}	heater surface area, [m^2]
c_p	specific heat, [kJ/kg.K]
D_H	channel hydraulic diameter, [m]
g	gravitional acceleration, [m/s^2]
Gr	Grashof number, [$=(g\beta(T_s-T_{inlet})_{ave.}D_H^3)/\nu^2$]
Gr*	modified Grashof number, [$=(g\beta\dot{q}_{conv.ave.}D_H^4)/k\nu^2$]
h	convection heat transfer coefficent, [$W/m^2.K$]
k	thermal conductivty, [W/m.K]
L	distance between heater and neighbour temperature, [m]
$L_{glasswool}$	glasswool insulation thickness, [m]
L_P	interplate distance, [m]
$\dot{m}$	mass flow rate of air, [kg/s]
N_{fan}	theoretical fan power, [W]
$Nu_{row\ ave.}$	row average Nusselt number, [$=(\dot{q}_{conv\ row\ ave}D_H)/(k(T_s-T_{inlet})_{row\ ave.})$]
P_{atm}	atmospheric pressure, [Pa]
P_c	channel perimeter, [m]
$\dot{q}_{conv.}$	convection heat flux, [W/m^2]
$\dot{q}_{conv\ ave.}$	all heaters average convection heat flux, [W/m^2]
$\dot{q}_{conv\ row\ ave}$	row average convection heat flux, [W/m^2]
$\dot{Q}_{electric}$	supplied electrical power, [W]

$\dot{Q}_{conv}$	convection heat transfer rate, [W]
$\dot{Q}_{cond.isolation}$	conduction heat transfer rate heater to isolation, [W]
$\dot{Q}_{cond.side}$	conduction heat transfer rate heater to side walls, [W]
$\dot{Q}_{rad}$	radiation heat transfer rate, [W]
R_{heater}	heater electrical resistance, [Ω]
R_{total}	total electrical resistance, [Ω]
Re	Reynolds number, [$=(w_{inlet}D_H)/\nu$]
Ri	Richardson number, [$=Gr/Re^2$]
T	fluid temperature, [K]
T_s	heater surface temperature, [K]
T_b	bulk temperature, [K]
T_{inlet}	air inlet temperature, [K]
u	x component of air velocity, [m/s]
v	y component of air velocity, [m/s]
V	voltage drop, [V]
w	z component of air velocity, [m/s]
w_{inlet}	air velocity at inlet, [m/s]
ρ	air density, [kg/m^3]
α	angle of plate, [degree]
β	thermal expansion coefficent, [1/K]
ν	kinematic viscosity, [m^2/s]
μ	dynamic viscosity, [kg/ms]
ϵ	heater surface emissivity
σ	Stefan-Boltzman constant, [W/m^2.K^4]

INTRODUCTION

The chips on the printed-circuit boards (PCBs) are presented as rectangular heat sources in many numerical and experimental studies in literature over the cooling of the electronic devices and increasing the heat transfer rate. In these studies, the effects of various flow conditions, channels and placement arrays of the heat sources on the temperature distribution and heat transfer were investigated. Wu and Perng (2008) investigated the mixed convection heat transfer from protruded heat sources in a horizontal channel numerically by placing a rectangular plate vertically into the entrance of the channel. The results show that the heat transfer enhancement is provided with the placement of plate for different parameters as Reynolds and Grashof number. The forced convection heat transfer from heat sources on the bottom surface of a horizontal channel, and a triangular shaped plate placed at the entrance of the channel were investigated by Oztop *et al.* (2009). It is obtained that insertion of triangular plate enhanced heat transfer and the highest heat transfer is observed at the position of the plate with y=3,5. Korichi *et al.* (2009) made a numerical analysis in a case when plates were placed periodically on the top surface of a channel which had three vertical protruded heat sources on the bottom surface. It is observed that different physical arrangement as plate lengths, angles affect heat transfer. Fu and Tong (2009) investigated the heat transfer from the heat sources in a case when a vibrating cylinder was placed into the entrance of a channel which had four vertical protruded heat sources on the bottom surface. Numerical results show that heat transfer enhancement occurs with the insertion of the cylinder for the variable cylinder vibration amplitudes and frequencies. The effects of the inclination angle and the thickness of a plate which placed into the channel on the heat transfer and pressure drop for unsteady flow conditions were investigated numerically by Davidson (2001). It is observed that heat transfer is variational for different solution methods. In a numerical study performed by Sohankar (2007), the effects of the plate angle and channel height on heat transfer and pressure drop was investigated by placing a V-shaped plate on the bottom surface of a rectangular and horizontal channel. The study shows that heat transfer and pressure drop increases with V-shaped plate and, DNS and LES simulation results are similar. Literature survey shows that using of flow routing objects (plates, cylinders, etc.) in the channel, affects heat transfer in different ratios based on the parameters as placement order of the heat sources, plate angle, plate length and thickness, Re and Gr numbers, or ratio of channel height to width. (Myrum *et al.*, 1993; Valencia, 1999; Chompookham *et al.*, 2010; Fu *et al.*, 2001; Beig *et al.*, 2011; Perng *et al.*, 2012; Wu and Tao, 2008; Fu *et al.*, 2012; Yang, 2002; Min *et al.*, 2012; Sripattanapipat and Promvonge, 2009; Teamah *et al.*, 2011)

There are not detailed analyses on the effects of the placement of flow routing plates on the mixed convection heat transfer in the channels that have heat sources on the bottom and top surfaces in the literature. In this present research, the heat transfer and the temperature distribution that occur when plates are placed into a horizontal channel which has protruded heat sources on the bottom and top surfaces were investigated numerically and experimentally. Also, the effects of the using of flow routing plate on heat transfer enhancement were analysed by comparing the cases with and without plate in the channel.

EXPERIMENTAL SET-UP

The experimental set-up is seen in Figure 1 mainly consists of a fan, a flow straightener, test zone, damping chamber to separate the test zone from the fan, DC power supply, and control panel, and measurement systems. The test zone has totally 64 protruded heat sources which are equipped with 4x8 rows on lower and upper walls, and there are two plates in the entrance of the test zone.

The test zone is a rectangular-shaped channel in a length of 500 mm with heater blocks and plates. The aluminium heater blocks which have 5 mm thickness, are manufactured by casting method and their surfaces are grinded. Resistance heaters are placed into the each aluminium blocks for heat generating. The parts of the channel that are 850 mm before the test zone and 150 mm after the test zone are composed to maintain the flow to be independent of the effects of the entrance and the exit of the channel respectively. The plates are placed on the line

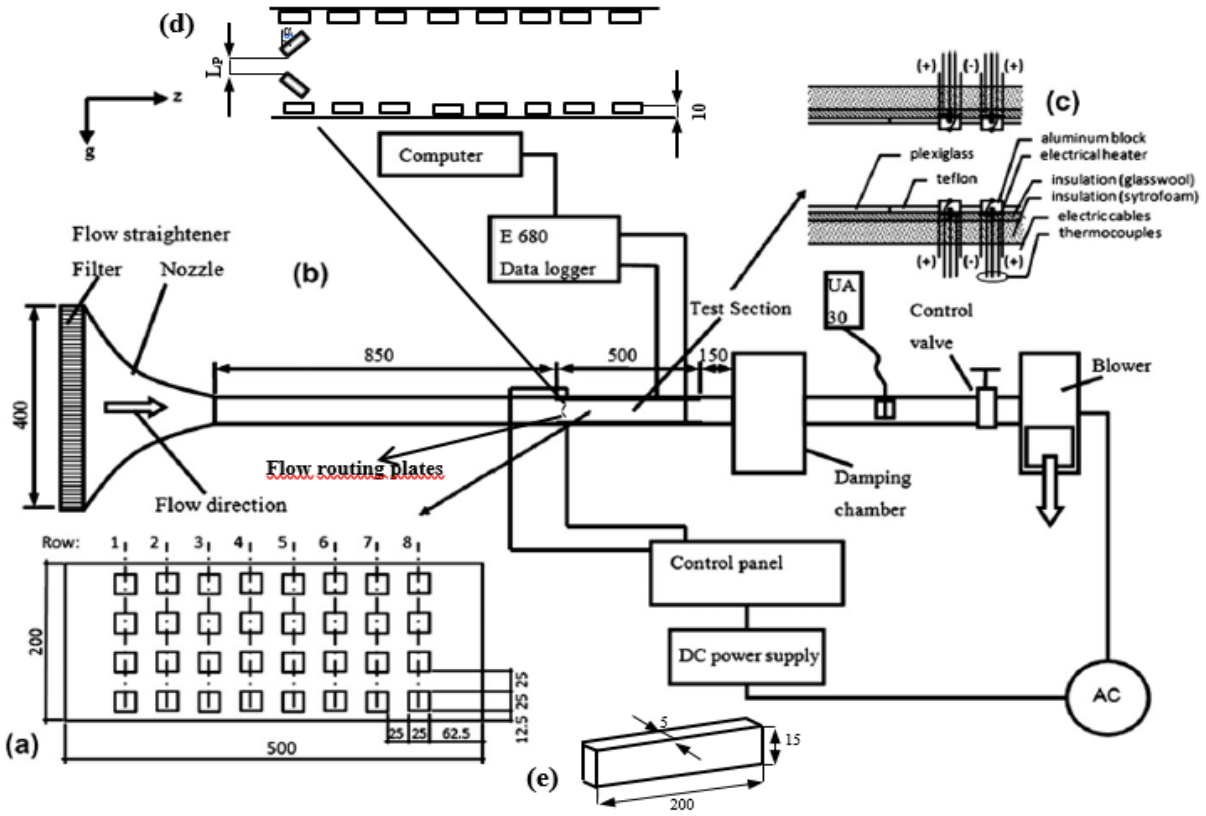

Figure 1. Schematic diagram of the experimental set-up (dimensions in mm.) a) Dimension of test zone (x-z plane), b) Experimental set-up, c) Schematic of heat sources assembly, d) Layout of plates (y-z plane) and e) Dimension of plexiglass plate.

of the first heater rows that are on the lower and upper surfaces. The dimensions of the test zone made from transparent plexiglas are shown in Figure 1.

There are holes which create $\alpha=30^{\circ}$ angle against the y-axis on the side walls of the channel for the placement of routing. Entire surface is produced from plexiglass material except the test zone where there are the heat sources and plates. Politetrafloroetilen material (PTFE) with a thickness of 5mm however, is used for the test zone. The outer surface of the channel is insulated with foam board that has a thickness of 50 mm. An insulation material (glass wool) with a thickness of 20 mm is placed between the heaters and the foam board to prevent the foam board material from being damaged by the effects of high values of temperature. There are thermocouples in both sides of the insulation material which are in the same alignment with the blocks as shown in Figure 1 to determine the heat transfer from the heater blocks to the insulation material.

A DC power supply and a control panel are used to get the necessary electric current for the heaters in the experiments. The necessary electric current values are obtained by changing the resistance from the control panel. Also, the control panel was equipped with low voltage adjustable regulators. These regulators are used for adjusting heater voltages with an accuracy of ±1%.

The flow straightener which consists of hoses in the diameter of 5 mm and the length of 50 mm is placed at the entrance of the channel to provide uniform velocity distribution in the channel. Also, it consists of a nozzle to eliminate flow separation and provide a uniform velocity profile. The nozzle is made of alloy plates with a thickness of 0,5 mm. The damping chamber is used to separate the test zone from the fan mechanically and acoustically, and to provide the fluid absorption of the fan to be uniform.

Measurement of the electric current, resistance and voltage drop necessary for the calculations, the Protek 506 digital multimeter is used with an accuracy of ±0.1% for the voltage, and of ±0.5% for the resistance. 201 copper-constantan (T-type) thermocouples are used for the measuring of temperatures. All thermocouples are separately calibrated. The outlets of the thermocouples are connected to the ELİMKO 680 series universal data loggers which have computer interaction. The thermocouples are also used in the inlets and outlets of the channel, and on some specific parts of the insulation for the heat transfer calculations. For the measurement of the flow velocity during the experiments, an airflow UA30 ultrasonic anemometer which can measure the speed in the range of 0-30 m/s was used with an accuracy of ±1%. It is observed that experimental conditions reach a steady state after approximately 4-6 h. The steady-state conditions are accepted to have been occurred when the variation of the temperature reaches to a negligible level($\Delta T < 0.1^{\circ}C$).

Processing of Experimental Data

The nondimensional parameters affecting the heat transfer and temperature distributions are calculated by using the equations given below.
The Re number was determined with Eq. (1),

$$Re=\frac{w_{inlet}D_H}{\nu} \quad (1)$$

In this equation, w_{inlet} shows the inlet velocity of the air entering the channel, and it is measured during the experiments. The kinematic viscosity of the air is shown by ν . D_H, hydraulic diameter is calculated from

$$D_H=\frac{4A_c}{P_c} \quad (2)$$

where A_c shows the cross-sectional area of the channel and P_c shows the channel perimeter.

Grashoff number (Gr) is calculated by the equation below,

$$Gr=\frac{g\beta(T_s-T_{inlet})_{ave.}D_H^{\,3}}{\nu^2} \quad (3)$$

where T_s is the surface temperature of the heater, T_{inlet} is the inlet temperature of the air entering the channel, g is the gravitational acceleration, β is the thermal expansion coefficient of the air at inlet conditions. The $(T_s-T_{inlet})_{ave}$ value is determined by considering the average temperature difference of the 64 heaters.

The modified Grashof number (Gr*) is calculated by using Eq. (4).

$$Gr^*=\frac{g\beta\,\dot{q}_{conv.ave.}\,D_H^{\,4}}{k\nu^2} \quad (4)$$

The $\dot{q}_{conv.\ ave.}$ is the average convection heat flux value for the 64 heaters, and k is the thermal conductivity of the air. The average convection heat flux value is calculated by finding the average value after the calculation of the convection heat flux value ($\dot{q}_{conv.}$) for each heater by using the equation given below.

$$\dot{q}_{conv.}=\frac{\dot{Q}_{conv.}}{A_{heater}} \quad (5)$$

where $Q_{conv.}$ is the convection heat transfer rate from each heater, and A_{heater} is the surface area of each heater.

The row average Nusselt number ($Nu_{row\ ave.}$) is calculated as given below,

$$Nu_{row\ ave.}=\frac{hD_H}{k} \quad (6)$$

where h is the convection heat transfer coefficient of the air and is calculated by Eq. (7).

$$h=\frac{\dot{q}_{conv.row\ ave.}}{(T_s-T_{inlet})_{row\ ave.}} \quad (7)$$

In this equation, $\dot{q}_{konv.row\ ave.}$ is the average convection heat flux that is obtained for each heater row consisting of four heater blocks, and $(T_s-T_{inlet})_{row\ ave.}$ is the average temperature difference. The Eq. (8) for the $Nu_{row\ ave.}$ is obtained by substituting the Eq. (7) into Eq. (6).

$$Nu_{row\ ave.}=\frac{\dot{q}_{conv.row\ ave.}D_H}{k(T_s-T_{inlet})_{row\ ave.}} \quad (8)$$

The Richardson number (Ri) is defined depending upon the Re and Gr numbers with the equation below,

$$Ri=\frac{Gr}{Re^2} \quad (9)$$

The expression of energy balance (Eq. 10) is used to identify the convection heat transfer rate.

$$\dot{Q}_{conv.}=\dot{Q}_{electric}-\dot{Q}_{cond.isolation}-\dot{Q}_{cond.side}-\dot{Q}_{rad.} \quad (10)$$

In the equation, $\dot{Q}_{electric}$ is the supplied electrical power, $\dot{Q}_{cond.insulation}$ is the conduction heat transfer rate from the heater to isolation, $\dot{Q}_{cond.side}$ is the heat transfer rate from heater to other heaters and side walls, and $\dot{Q}_{rad.}$ is the heat transfer from the heaters with radiation.

Supplied electrical power ($\dot{Q}_{electric}$) is calculated with the equation below by using the voltage drop in the heaters (V), and the total resistance (R_{total}) which is the total resistance of the line between the control panel and the heater, and the heater resistance (R_{heater}).

$$\dot{Q}_{electric}=\frac{V^2R_{heater}}{R^2_{total}} \quad (11)$$

Conduction heat transfer rate from heater to glass wool isolation ($\dot{Q}_{cond.insulation}$) however, is calculated from,

$$\dot{Q}_{cond.isolation}=\frac{k_{isolation}A(T_{top}-T_{bottom})}{L_{isolation}} \quad (12)$$

where $k_{isolation}$ is the thermal conductivity of the glass wool insulation, $L_{isolation}$ is the thickness of the glass wool insulation, and A is the heat transfer area. The expression of $(T_{top} - T_{bottom})$ is the temperature difference for the insulations of the bottom and top surfaces.

The heat transfer rate ($\dot{Q}_{cond.side}$) from the heater to the other heaters or side walls is calculated from

$$\dot{Q}_{cond.side} = \frac{k_{teflon} A(T_{heater} - T_{neighbour})}{L} \quad (13)$$

where T_{heater} is the heater temperature measured, $T_{neighbour}$ is the either neighbouring heater temperature when there is heat transfer between the heaters, or is the edge temperature in case there is heat transfer to the edges of the teflon. In calculating the edge temperatures, bulk temperatures, and the temperature distribution in the foamboard are taken into account. The k_{teflon} is the thermal conductivity of the teflon plate, and L is the distance between the heater and the point where the neighbouring temperature value is taken.

Eq. (14) is used to calculate the radiation heat transfer rate ($\dot{Q}_{rad.}$).

$$\dot{Q}_{rad.} = \sigma \varepsilon F A_{heater} (T_s^4 - T_b^4) \quad (14)$$

where σ is the Stefan-Boltzmann constant, ϵ is the emissivity of the aluminium heater blocks, T_s is the surface temperature of the heaters, and T_b is the average bulk temperature of the fluid. The F shape factor is taken as F=1.

The bulk temperatures T_b can be calculated by applying the principle of the conservation of energy to a selected control volume in the channel (Eq. (15)). The selected control volume includes each four heaters on the lower and upper surfaces for a heater row. Air is used as a cooling fluid and it is accepted as an ideal gas.

$$T_{b2} = \frac{\dot{Q}_{total.c.v.}}{\dot{m} c_P} + T_{b1} \quad (15)$$

In this equation, $\dot{m}$ is the mass flow rate of the air, c_p is the specific heat, T_{b1} is the inlet temperature of the air before the heater row (it is the inlet temperature of the fluid entering the channel for the first heater row), and T_{b2} is the inlet temperature of the air before the next heater row. $\dot{Q}_{total.c.v.}$ is the total heat energy amount transferred to the fluid from the 8 heaters in the control volume. All the thermophysical properties of the air are defined at the bulk temperature.

The standard calculation methods in the literature are used for uncertainty analysis of the experimental results (Moffat, 1982; Kline, 1985; Smith and Wehofer, 1985). The uncertainty in the Nusselt number is calculated around ±5% depending upon uncertainties of $\dot{q}_{konv.row\ ave.}$, D_H, k and $(T_s - T_{inlet})_{row\ ave.}$. The uncertainties of modified Grashof number and Re number, however, are calculated around ±3% depending upon uncertainties of D_H, k and $\dot{q}_{conv.\ ave..}$ and around ±2% depending upon uncertainties of D_H and w_{inlet}, respectively.

NUMERICAL STUDY

The problem analysed in the numerical study includes the effects of using of flow routing plates on heat transfer from protruded heat sources in a three-dimensional channel. Numerical analysis is performed by creating a mathematical model, and the numerical findings obtained are compared to the experimental findings to make validation of numerical results. Geometries used in the numerical study for the cases with and without plate are seen in Figure 2. Dimensions of these geometries are identical with Figure 1.

Mathematical Model

The air was used as the cooling fluid, and analyses were performed by assuming the fluid is Newtonian, incompressible, and convection properties of the fluid are constant for the steady-state and laminar flow conditions. Also, the Boussinesq approach was used to determine the effects of the buoyant force. The conservation equations given below were used to calculate the air velocity components (u, v, w), the pressure (P) and temperature (T) values in the study.

The conservation of mass equation is expressed with the Eq. (16).

$$\frac{\partial(\rho u)}{\partial x} + \frac{\partial(\rho v)}{\partial y} + \frac{\partial(\rho w)}{\partial z} = 0 \quad (16)$$

The conservation of momentum equations is expressed with the equations given below in the directions of x, y and z respectively.

$$u\frac{\partial(\rho u)}{\partial x} + v\frac{\partial(\rho u)}{\partial y} + w\frac{\partial(\rho u)}{\partial z} = -\frac{\partial P}{\partial x} + \mu\left(\frac{\partial^2 u}{\partial x^2} + \frac{\partial^2 u}{\partial y^2} + \frac{\partial^2 u}{\partial z^2}\right) \quad (17)$$

$$u\frac{\partial(\rho v)}{\partial x} + v\frac{\partial(\rho v)}{\partial y} + w\frac{\partial(\rho v)}{\partial z} = -\frac{\partial P}{\partial y} + \mu\left(\frac{\partial^2 v}{\partial x^2} + \frac{\partial^2 v}{\partial y^2} + \frac{\partial^2 v}{\partial z^2}\right) + \rho g \beta (T - T_{inlet}) \quad (18)$$

$$u\frac{\partial(\rho w)}{\partial x} + v\frac{\partial(\rho w)}{\partial y} + w\frac{\partial(\rho w)}{\partial z} = -\frac{\partial P}{\partial z} + \mu\left(\frac{\partial^2 w}{\partial x^2} + \frac{\partial^2 w}{\partial y^2} + \frac{\partial^2 w}{\partial z^2}\right) \quad (19)$$

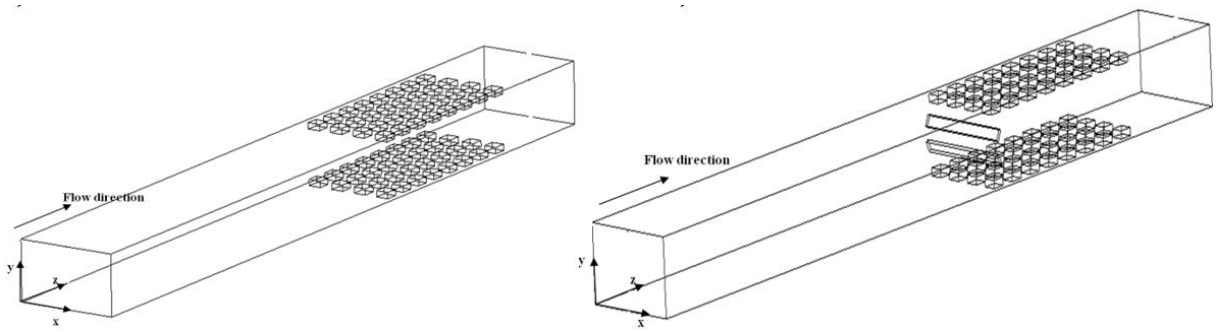

a) b)

Figure 2. Geometries for the numerical analyses a) the case without plate b) the case with plate

In the differential equations given above u, v and w is the velocity components in the direction of x, y and z respectively, P is the pressure, μ is the dynamic viscosity of the fluid, ρ is the density of the fluid, g is the gravitational acceleration, β is the thermal expansion coefficient of the fluid at inlet temperature, T is the fluid temperature, and T_{inlet} is the inlet temperature of the fluid. The last expression on the right side of the Eq. (18) is used for the purpose of identifying the effects of mass forces (Boussinesq approach).

The conservation of energy equation can be written as follows.

$$u\frac{\partial(\rho T)}{\partial x}+v\frac{\partial(\rho T)}{\partial y}+w\frac{\partial(\rho T)}{\partial z}=\frac{k}{c_p}\left(\frac{\partial^2 T}{\partial x^2}+\frac{\partial^2 T}{\partial y^2}+\frac{\partial^2 T}{\partial z^2}\right) \quad (20)$$

where c_p is the specific heat of the fluid, and k is the thermal conductivity of the fluid.

The boundary conditions in the inlet and the outlet of the channel are given in Eq.(21) and (22) respectively.

$u = 0; v = 0; w = w_{inlet}; T_{inlet}=23{,}5°C;$

$$P_{atm}=101325\ Pa \quad (21)$$

$$\frac{\partial u}{\partial z}=0\ ;\ \frac{\partial v}{\partial z}=0\ ;\ \frac{\partial w}{\partial z}=0\ ;\ \frac{\partial T}{\partial z}=0 \quad (22)$$

The flow is symmetrical to the axis of x. Therefore, the boundary conditions in the symmetrical axis of the channel can be written as follows;

$$u=0;\ \frac{\partial v}{\partial x}=0\ ;\ \frac{\partial w}{\partial x}=0\ ;\ \frac{\partial T}{\partial x}=0\ ;\ \frac{\partial P}{\partial x}=0 \quad (23)$$

No-slip conditions were defined on the lower, upper and side surfaces of the channel, over the plates and heat sources and all surfaces were assumed to be adiabatic except surface of heat sources;

$$u = 0;\quad v = 0;\quad w = 0;\quad \dot{q} =0 \quad (24)$$

The boundary condition identified on the heater surfaces is given in Eq. (25);

$$\dot{q}=\dot{q}_{conv.} \quad (25)$$

Numerical Method

Creating the geometries and numerical analyses were performed by the ANSYS Fluent (2011) software for the problem. The channel model was created depending upon the measures in Figure 1. As the flow in the channel was symmetrical to the middle of the channel in the direction of x-axis, half of the geometry given in Figure 2 was modelled.

The SIMPLE and Coupled algorithm with the option of Pseudo-Transient were adopted to derive the discretized form of all conservation equations are given Eq. (16)-(20) in the case with and without plate respectively. The Second Order Upwind Differencing scheme was adopted for discretizing terms in Eq. (16)-(20). The iterations were maintained until the residual values became less than $1x10^{-6}$ for the conservation of mass and momentum, and less than $1x10^{-10}$ for the energy equations.

Processing of Numerical Data

Numerical analysis was carried out by assuming uniform and constant heat flux values ($\dot{q}_{conv.}$) for each heater block and values of heat fluxes that calculated with Eq.(5) during the experiments, are used for comparing of experimental and numerical results. The Re number, Gr number, modified Gr number (Gr*), row average

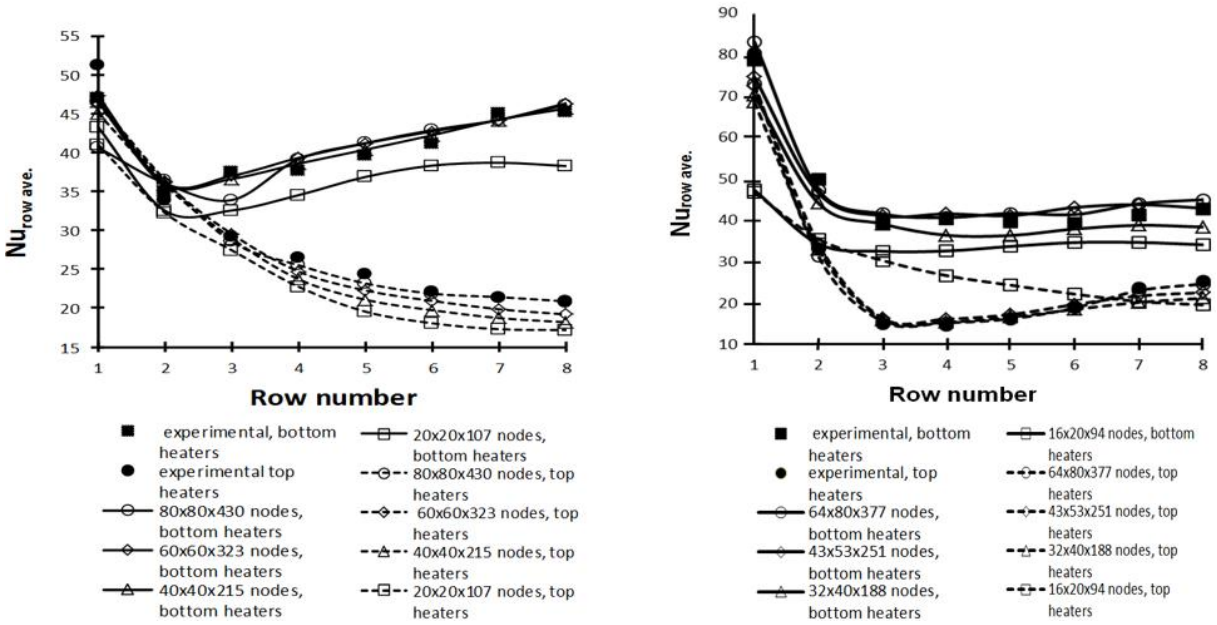

a) **b)**

Figure 3. Grid independent test results for different numbers of node (Re=2000, $Gr^*=3x10^8$, α=30˚, $L_P/H=3/20$, H/W=1/2) a) without plate b) with plate

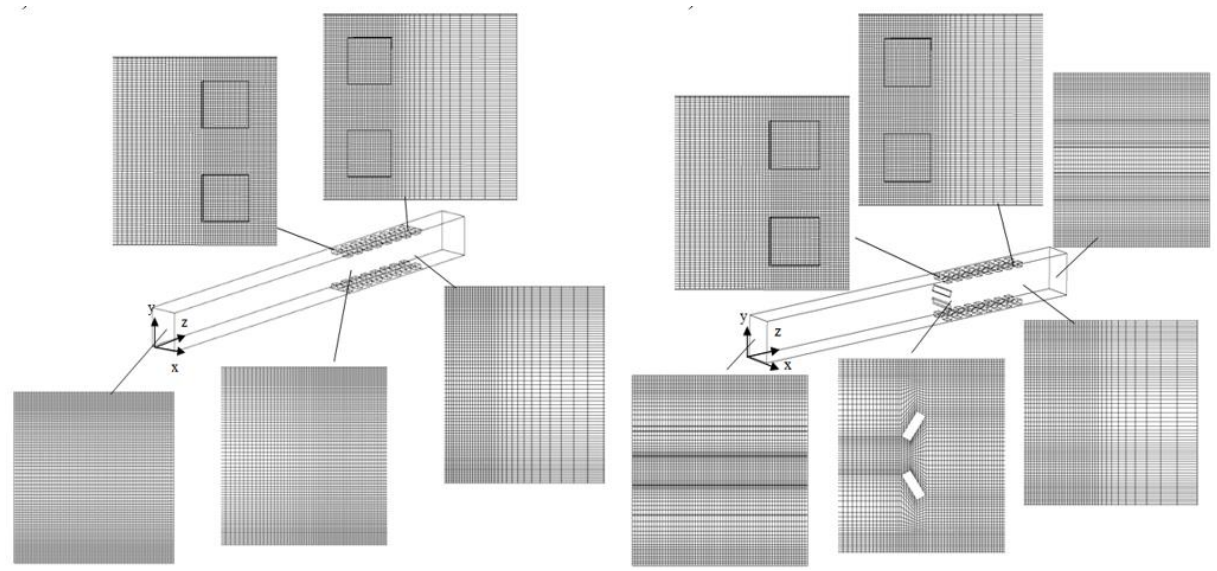

a) **b)**

Figure 4. Mesh structure and distribution a) without plate b) with plate(α=30˚)

Nusselt number and Ri number, however, are calculated with Eq. (1),(3),(4), (8) and (9) respectively.

Validation of Numerical Data

In order to obtain grid independent solutions and compatible results with experiments, a grid independent test was carried out. A uniform grid was used for throughout the domain but a fine grid was used near the walls. Grid independent test results for different numbers of node are presented in Figure 3. As seen in Figure 3., it is observed that the mesh structures with 64x80x377 and 80x80x430 nodes on the x, y and z-axes are in compliance with experimental results for the cases with and without plate, respectively.

The mesh structure and distribution for the cases with and without plate are shown in Figure 4. The comparisons of the experimental and numerical study results for the row average Nusselt numbers in the value of two different Reynolds numbers for the cases without and with plate are shown in Figure 5 and 6 respectively. As can be seen from these figures, there is a very good agreement between the numerical and experimental results. The maximum difference between experimental and numerical values does not exceed 7%. This can be

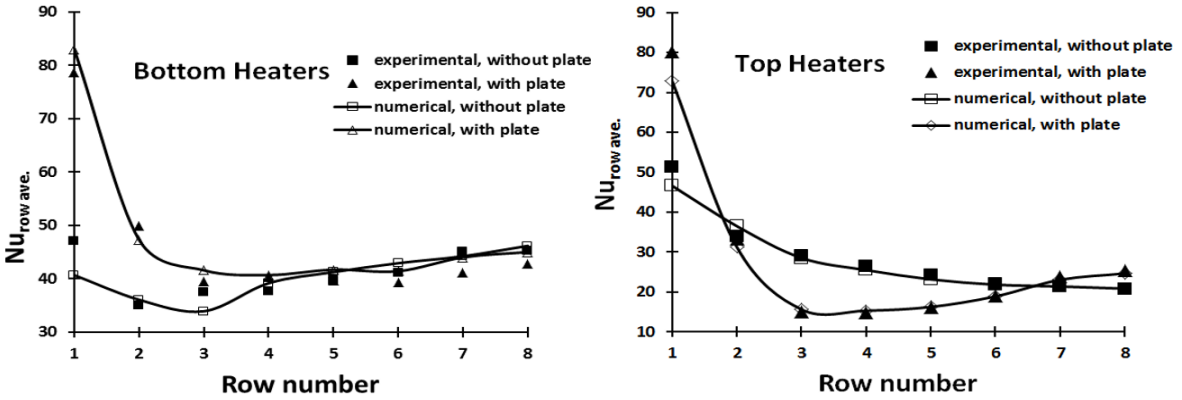

Figure 5. Comparison of experimental and numerical results (α=30˚, Gr*=3x10^8, Re=2000, H/W=1/2, L_P/H=3/20)

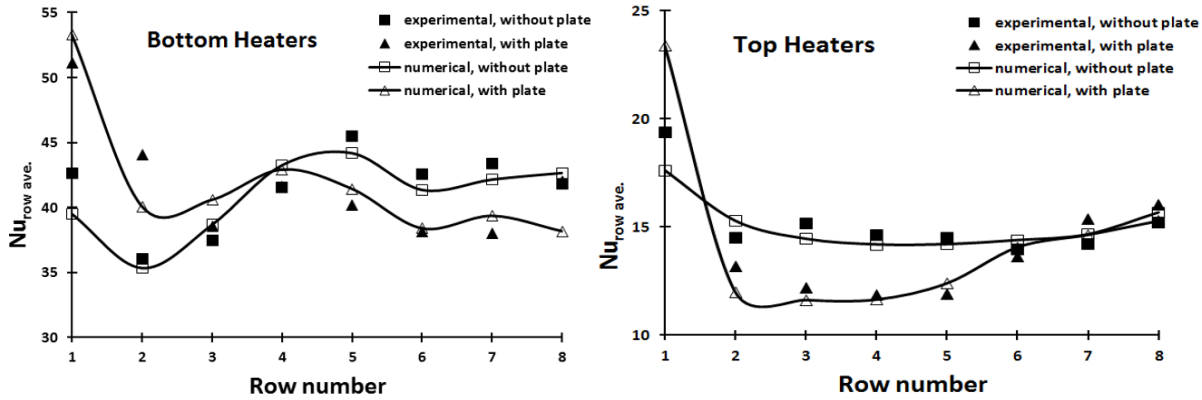

Figure 6. Comparison of experimental and numerical results (α=30˚, Gr*=3x10^8, Re=930, H/W=1/2, L_P/H=3/20)

considered as a sufficient verification of the computational domain and numerical procedures applied in the present study.

RESULTS AND DISCUSSION

The experimental study was performed for certain Re and Gr* number values and compared to the numerical study of the same parametrical values. After this, a parametrical study was performed numerically for the different Re and Gr* numbers, and the values of the plate angles (α). The numerical study parameters are given in Table 1. The comparisons between the cases with and without plates for the row average Nu number and temperature difference at different Gr*, Re numbers and plate angles, are presented in Figures. 7 and 8.

Using plates increases the $Nu_{row\ ave.}$ at the first four heater rows for bottom heaters according to the case without plate (Figure 7a). As can be seen from Figure 6a, the heat transfer decreases with decrease in Gr* number. At all Gr* number values, the temperatures of the bottom heaters increase until a certain heater row and decrease due to the effect of buoyancy affected secondary flow.

The $Nu_{row\ ave.}$ distributions for the different Re numbers can be seen in Figure 7b. For all the values of Re numbers, it is observed that the heat transfer in the first four heater rows when there are plates is greater, and the heat transfer from other heaters decreases when compared to the case without plates. Using plates is only useful for the first four heater rows since the heat transfer decreases after the fifth heater row. On the other hand, the heat transfer enhancement increases with increase in Re number when all heater rows are taken into account.

Table 1. Numerical study parameters for the cases with and without plate

Re	Gr*	W_{inlet} (m/s)		Ri		L_P/H	H/W	α	Ri	α	Ri	α	Ri
2000	3 x 10^8	0,24	Without plate	1,9	With plate	3/20	1/2	0˚	2,7	30˚	2,2	60˚	2,3
2000	2 x 10^8	0,24		1,3		3/20	1/2	0˚	1,9	30˚	1,4	60˚	1,5
2000	1 x 10^8	0,24		0,76		3/20	1/2	0˚	1	30˚	0,7	60˚	0,8
1400	3 x 10^8	0,16		5,2		3/20	1/2	0˚	6,4	30˚	6,3	60˚	5,7
930	3 x 10^8	0,11		13,5		3/20	1/2	0˚	15,3	30˚	14,9	60˚	13,9

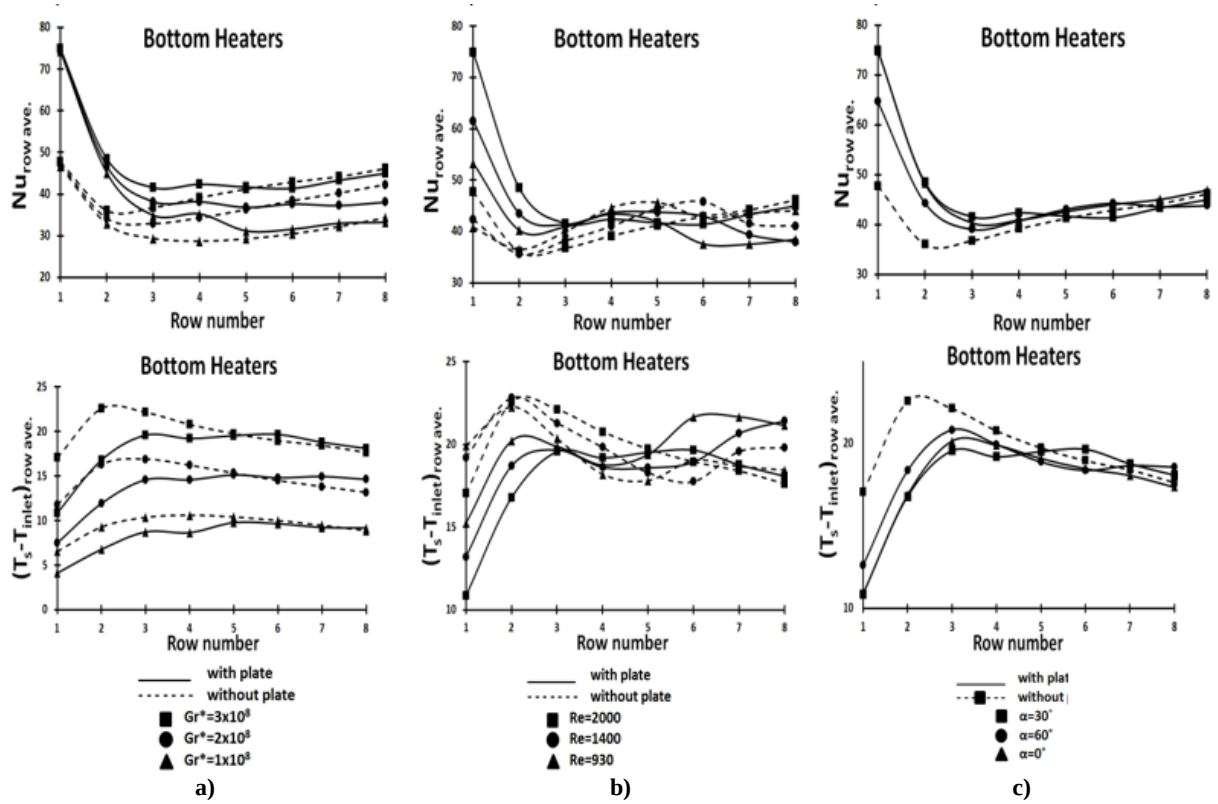

Figure 7. $Nu_{row\ ave.}$ and $(T_s-T_{inlet})_{row\ ave.}$ distributions at the bottom heaters a) for different Gr* numbers, b) for different Re numbers c) for different plate angles (α)

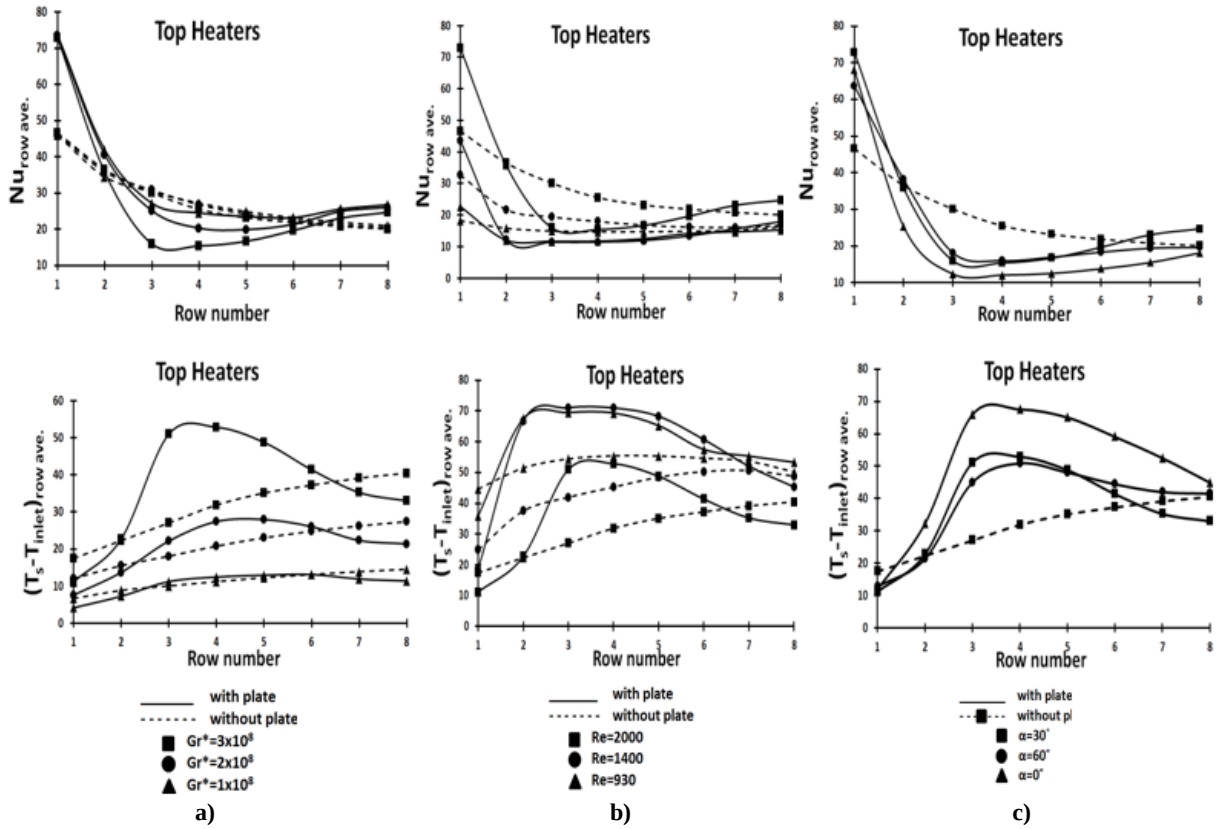

Figure 8. $Nu_{row\ ave.}$ and $(T_s-T_{inlet})_{row\ ave.}$ distributions at the top heaters a) for different Gr* numbers, b) for different Re numbers c) for different plate angles (α)

The $Nu_{row\ ave.}$ are higher than those of the case without plate until 5th heater row for the plate angles of α=30˚, 60˚, 0˚ (Figure 7c). After fifth heater row, however, there are not much difference in the heat transfer. When all the bottom heaters are considered, the highest heat transfer enhancement occurs for the plate angle of

α=30˚. When the bottom heater temperatures are considered, the heater temperatures increase until the 3rd heater row and then begin to decrease due to the effect of the natural convection for all plate angles.

$Nu_{row\ ave.}$ and temperature distributions at different Gr* numbers are shown in Figure 8a for the top heaters. Use of plate has only provided heat transfer enhancement at the first and the last heater row. There is a great amount of decrease in heat transfer at the 3rd-6th heater rows compared to the case without plate and the heat transfer increases with the decrease in the Gr* number for the case with plate. Temperatures of heater rows increase starting from the first heater row to the last heater one for the case without plate. Temperatures for the case with plate, however, increase until 4th heater row and then decrease up to the last one.

Effects of the Re number on the $Nu_{row\ ave.}$ and temperature distributions for the top heaters at the case with and without plate is observed in Figure 8b. The heat transfer enhancement for the first heater row and the last heater row occur after the placement of the plates at the Re numbers of Re=2000 and Re=1400. With the decrease of the Re number (Re=930), the heat transfer for the last two heater rows in the case with plate remains nearly the same as for the case without plate. The heat transfer for other heater rows decreases for the case with plate at all the Re numbers.

Distribution of row average Nu numbers and temperatures at various plate angles for the top heaters are given in Figure 8c. The heat transfer is higher only for the first heater row for the case with plate angle of α=0˚. The heat transfer enhancement occurs in different amounts for the first heater row for the cases of α=30°, 60° but for the last two heater rows when the angle is α=30. The heater temperatures increase until the 4th heater row for the plate angles of α=30°, 60° and 0˚, and then decrease after the 3rd heater row.

The velocity vectors and the temperature contours for the case with and without plate are given in Figure 9.The air accelerates while passing between the first heater row and the plates. The air also hits the top and bottom heater surfaces while passing through the between the plate and the heater and then turn towards the middle of the channel. This case causes that the adequate amount of air flow cannot reach to the 3rd – 6th heater rows, and thus the heat transfer decreases. Even though the adequate amount of flow cannot reach to the 3rd – 6th heater rows, the natural convection that occurs on the bottom heaters contributes to the cooling. The air ascends with the effect of buoyancy affected secondary flow and squeezes among the top heaters.

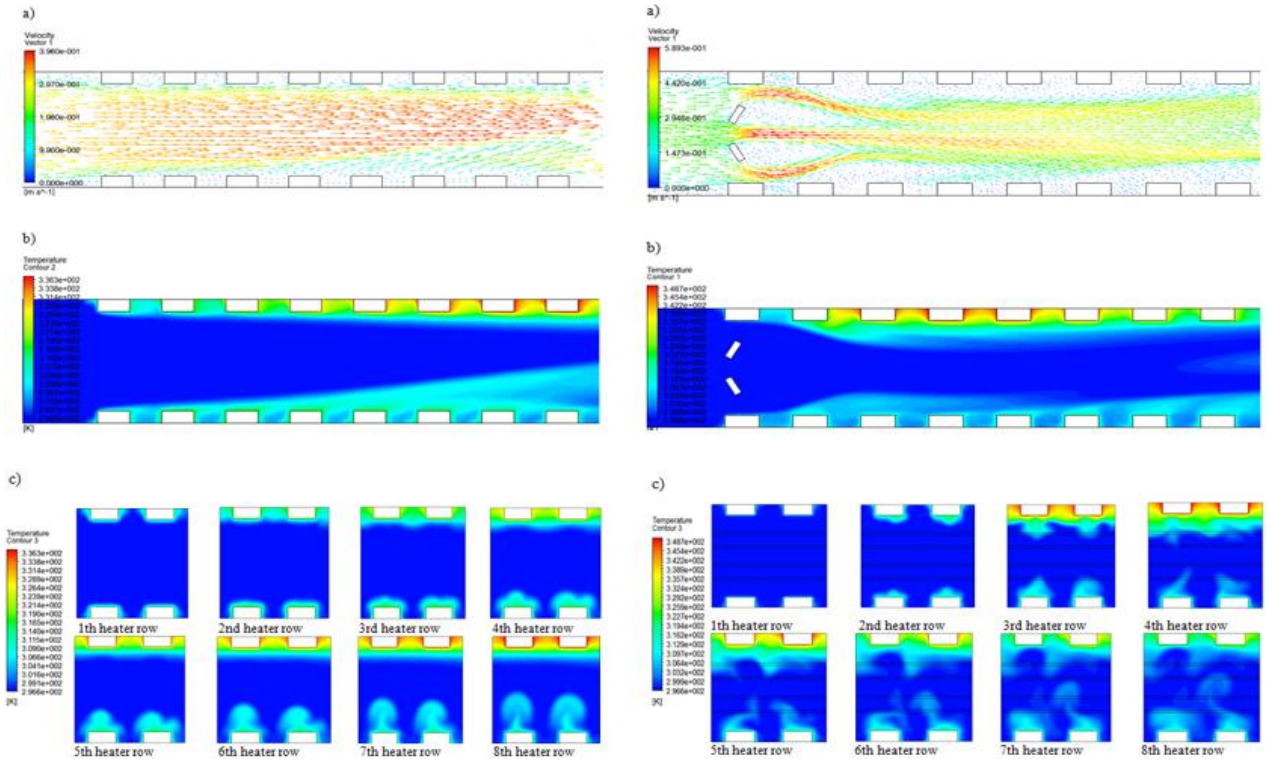

Figure 9. For the cases with and without plate, a) Velocity vectors at y-z plane, x=25mm, b) Temperature contours at y-z plane, x=25mm, c) Temperature contours at x-y plane (Re=2000, $Gr^*=3x10^8$, α=30˚, H/W=1/2, $L_P/H=3/20$)

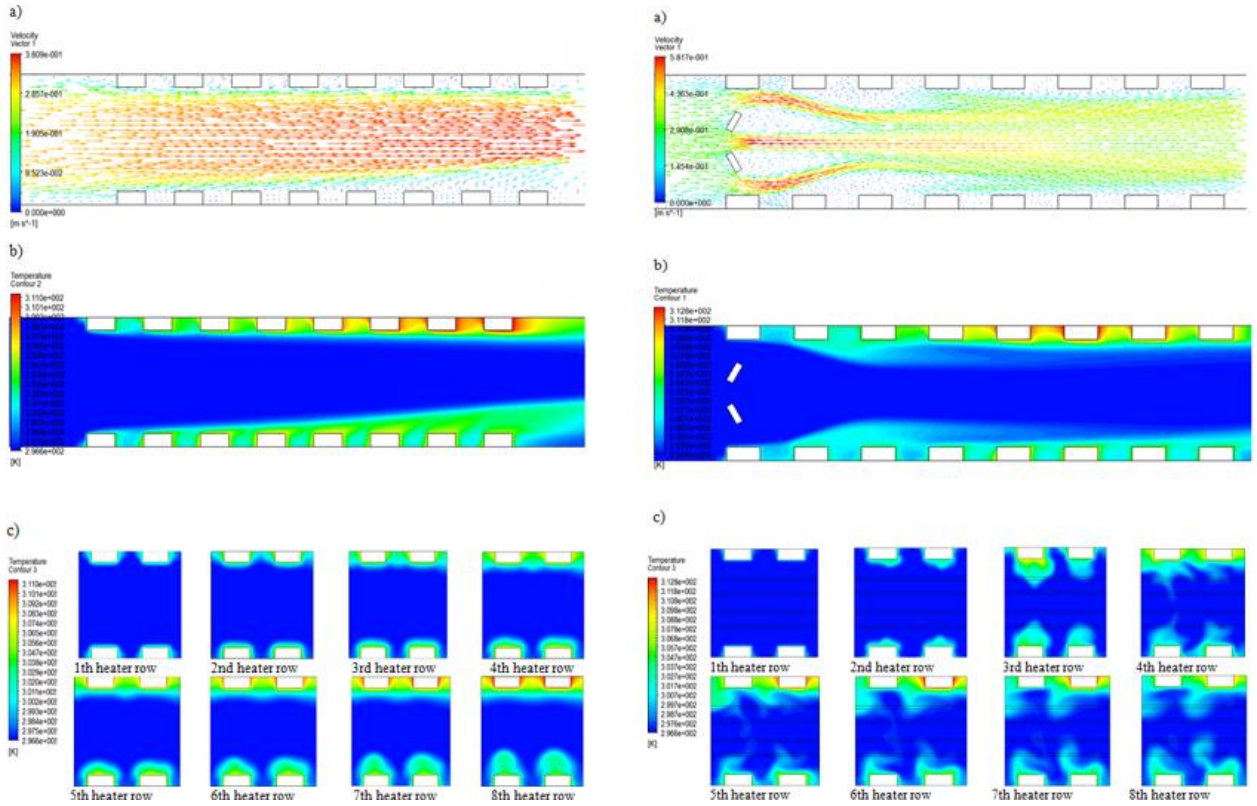

Figure 10. For the cases with and without plate, a) Velocity vectors at y-z plane, x=25mm, b) Temperature contours at y-z plane, x=25mm, c) Temperature contours at x-y plane (Re=2000, $Gr^*=1x10^8$, α=30˚, H/W=1/2, $L_P/H=3/20$)

Therefore, the heater temperatures increase more on the top heater rows. The air flow is more parallel to the bottom and top heater surfaces for the case without plate. This case provides preferable cooling conditions for only the top heaters. The temperatures of the bottom heaters decrease as the effect of buoyancy affected secondary flow increases throughout the last heater rows.

As seen from Figure 10, with the decrease of the Gr* number from $Gr^*=3x10^8$ to $Gr^*=1x10^8$, the Ri number takes the values of Ri=0,76 and Ri=0,7 depending upon the cases with and without plate, respectively and thus the forced convection condition becomes more dominant in the channel. The increase in the effect of forced convection causes a decrease in the effect of buoyancy affected secondary flow on the bottom heaters for both the cases. The top heater temperatures decrease due to the decrease in the amount of hot air that is squeezed among the heaters. Thus, the difference in the temperatures and the heat transfer rates between the cases with and without plate decrease.

The velocity vectors and temperature contours at different Re numbers for a specific Gr* number and plate angle are presented in Figure 11 and 12. Natural convection becomes more dominant with the decrease in the Re number for both cases with and without plate. The air flow passing through between the plate and the heater surface directs more to the middle of the channel especially for the top heaters by hitting the first heater row for the case with plate (Figure 11 and 12). In this case, the heater temperatures of 2nd -8th heater rows increase more compared to the case without plate. For the bottom heaters, the heat transfer after the 5th heater row at the case without plate is higher than those of the case with plate due to the effect of buoyancy affected secondary flow.

The velocity vectors and temperature contours depending on the variation of the plate angle are presented in Figure 13. For the angle of α=60°, the air that hits the top heater surfaces changes direction slightly since the distance between the plate and the heater surfaces is larger than those of the angle of α=30° and α=0°. This case creates greater cooling conditions for the second heater row on the top surface when compared to the cases which have plate angles of α=30° and 0˚. But because the air velocity in the entrance of the channel decreases in this angle, the heat transfer enhancement decreases for the first and last two heater rows compared the case with plate angle of α=30° and 0˚.

CONCLUSIONS

In the experimental and numerical analyses, it is investigated that using flow routing plates has only provided heat transfer enhancement for the first four

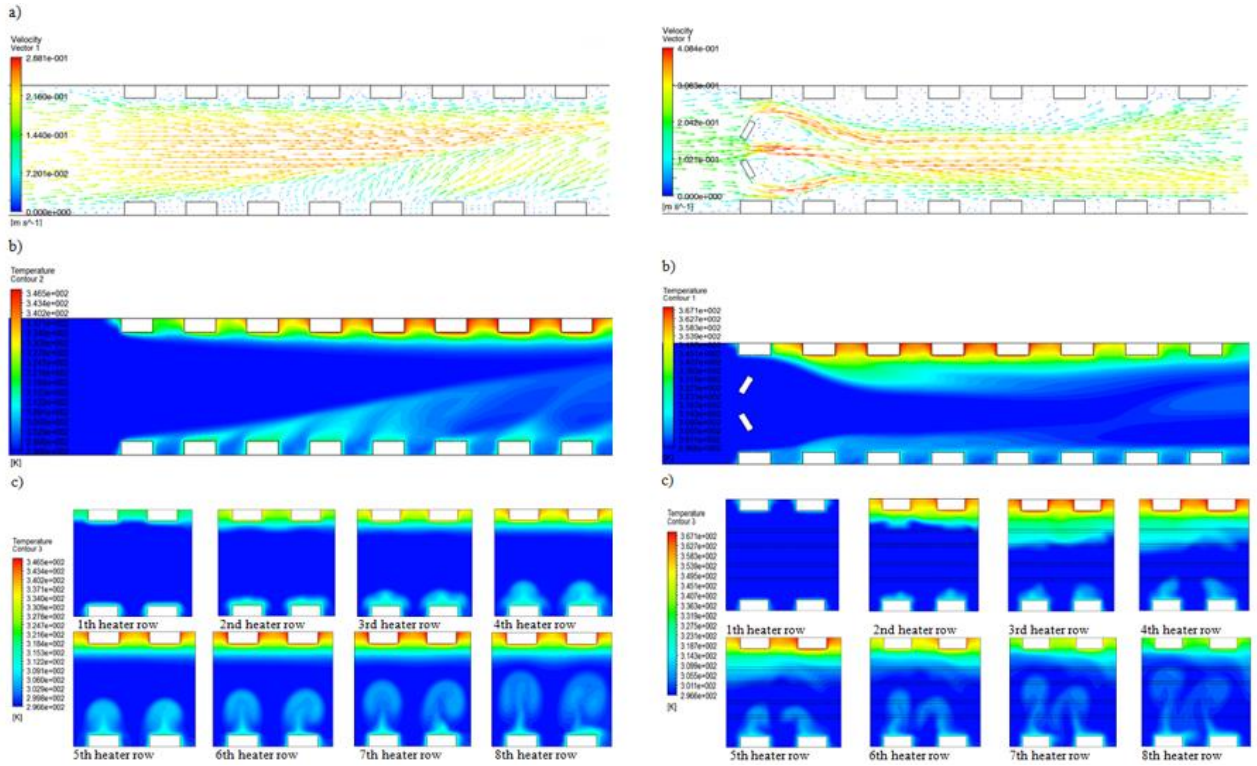

Figure 11. For the cases with and without plate, a) Velocity vectors at y-z plane, x=25mm, b) Temperature contours at y-z plane, x=25mm, c) Temperature contours at x-y plane (Re=1400, $Gr^*=3x10^8$, $\alpha=30^\circ$, H/W=1/2, $L_P/H=3/20$)

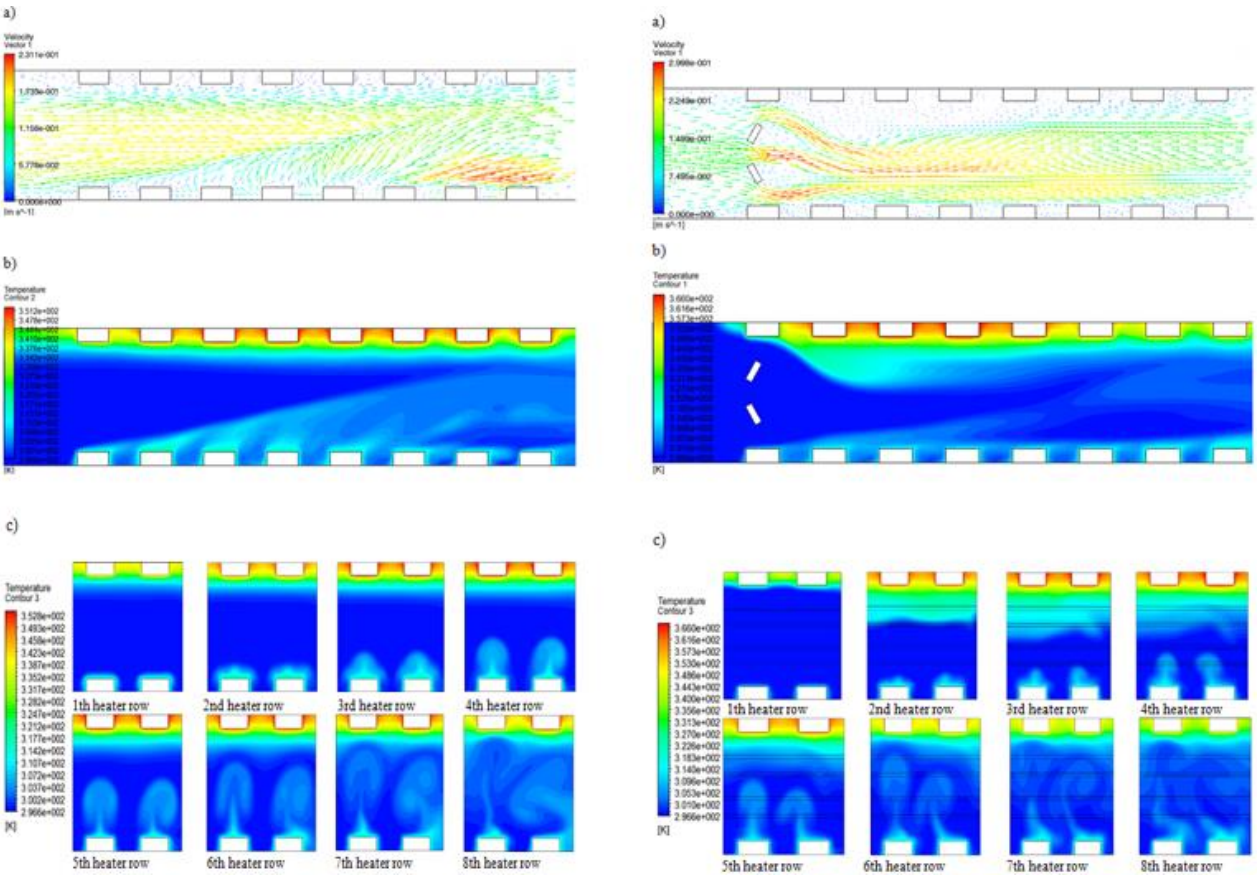

Figure 12. For the cases with and without plate, a) Velocity vectors at y-z plane, x=25mm, b) Temperature contours at y-z plane, x=25mm, c) Temperature contours at x-y plane (Re=930, $Gr^*=3x10^8$, $\alpha=30^\circ$, H/W=1/2, $L_P/H=3/20$)

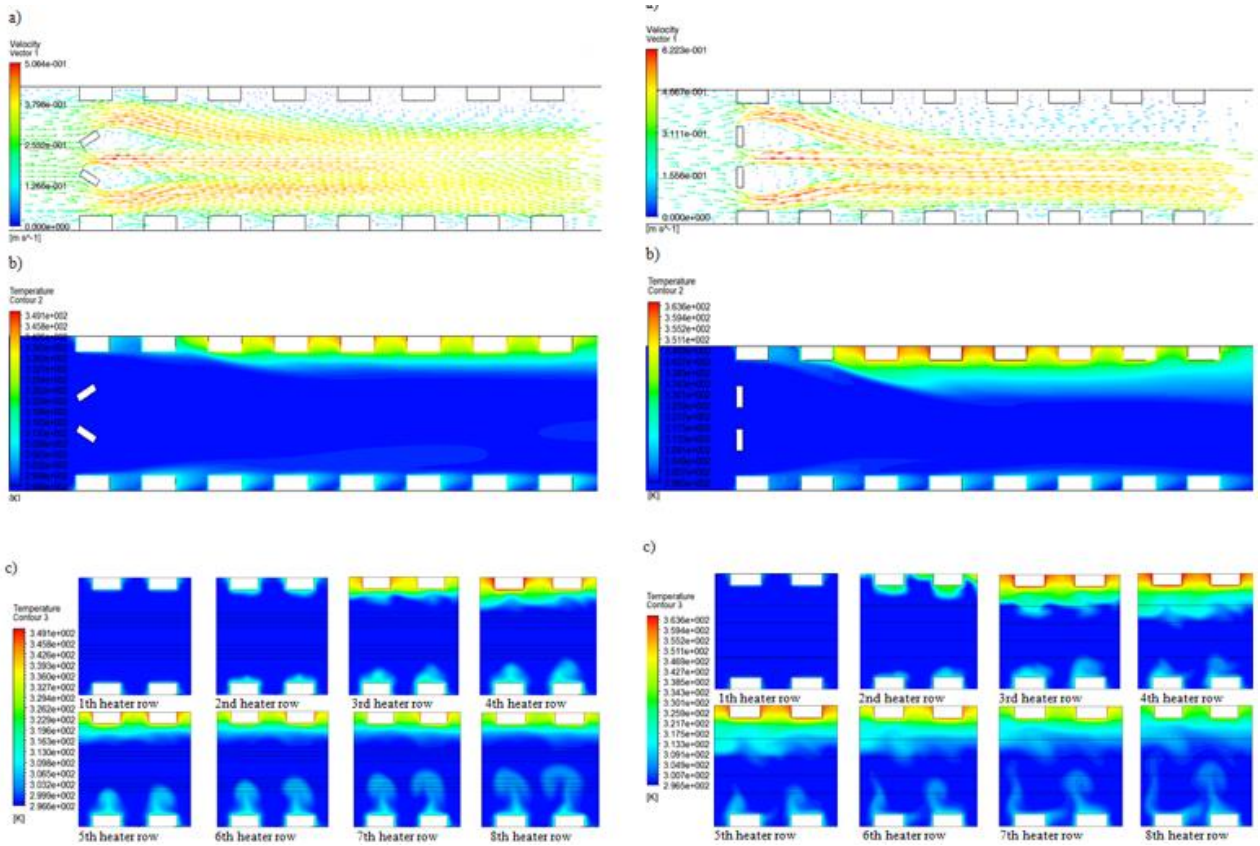

Figure 13. For the cases with plate (α=60˚,and α=0˚) a) Velocity vectors at y-z plane, x=25mm, b) Temperature contours at y-z plane, x=25mm, c) Temperature contours at x-y plane (Re=2000, $Gr^*=3x10^8$, H/W=1/2, $L_P/H=3/20$)

heater rows which are placed at the bottom surface, and the first and the last heater rows which are placed on the top surface. The air passing through between the plates and heaters hits the heater surface and directs to the middle of the channel. This causes the adequate amount of air flow cannot reach to the heater rows of 3rd-6th, and this also causes the decreasing of heat transfer when compared to the case without plate. Also, the air velocity that flowing between plates increases for high Re number and prevents increase in the amount of air that directing to the middle of the channel. For this reason, the air flow more directs to the middle of the channel at low Re number.

The natural convection increases with increase in Gr* number and decrease in Re number. Heated air rises and leaves the channel due to density difference between hot and cold air with increase in natural convection for the bottom heaters. This case increases heat transfer from bottom heaters. Effect of natural convection is different for the top heaters. Ascending hot air with the effect of buoyancy affected secondary flow squeezes among the top heaters. Therefore, the heater temperatures increase more on the top heater rows in regard to bottom heater rows.

Plate angle is the another important parameter and affects heat transfer in different ratios. Variation of plate angle changes the distance between plate and heater surface. The air accelerates while passing through the region between heater rows and plates. This situation increases heat transfer for certain heater rows. The distance between plate and heater surface is minimum for the angle of α=30˚. Thus, the highest heat transfer enhancement when compared to the case without plate is obtained at an angle of α=30˚.

REFERENCES

Beig, S. A., Mirzakhalili, E. and Kowsari, F., 2011, Investigation of optimal position of a vortex generator in a blocked channel for heat transfer enhancement of electronic chips, *International Journal of Heat and Mass Transfer*, 54(19), 4317-4324.

Chompookham, T., Thianpong, C. and Kwankaomeng, S., and Promvonge, P., 2010, Heat transfer augmentation in a wedge-ribbed channel using winglet vortex generators, *International Communications in Heat and Mass Transfer*, 37(2), 163-169.

Davidson, A. S. L., 2001, Effect of inclined vortex generators on heat transfer enhancement in a three-dimensional channel *Numerical Heat Transfer: Part A: Applications*, 39(5), 433-448.

FLUENT, A. 2011, Release 14.0, User Guide, Ansys. *Inc., Lebanon, US*.

Fu, W. S., Ke, W. W. and Wang, K. N., 2001, Laminar forced convection in a channel with a moving block, *International journal of heat and mass transfer*, 44(13), 2385-2394.

Fu, WS. and Tong, BH., 2004, Numerical investigation of heat transfer characteristics of the heated blocks in the channel with a transversely oscillating cylinder, *International Journal of Heat and Mass Transfer*, 47(2), 341-351.

Fu, W. S., Chen, C. J., Wang, Y. Y. and Huang, Y., 2012, Enhancement of mixed convection heat transfer in a three-dimensional horizontal channel flow by insertion of a moving block, *International Communications in Heat and Mass Transfer*, 39(1), 66-71.

Kline, S. J., 1985, The purposes of uncertainty analysis, *Journal of Fluids Engineering*, 107(2), 153-160.

Korichi, A., Oufer, L. and Polidori, G., 2009, Heat transfer enhancement in self-sustained oscillatory flow in a grooved channel with oblique plates, *International Journal of Heat and Mass Transfer*, 52(5), 1138-1148.

Min, C., Qi, C., Wang, E., Tian, L. and Qin, Y., 2012, Numerical investigation of turbulent flow and heat transfer in a channel with novel longitudinal vortex generators, *International Journal of Heat and Mass Transfer*, 55(23), 7268-7277.

Moffat, R. J., 1982, Contributions to the theory of single-sample uncertainty analysis. ASME, Transactions, *Journal of Fluids Engineering*, 104(2), 250-58.

Myrum, T. A., Qiu, X. and Acharya, S., 1993, Heat transfer enhancement in a ribbed duct using vortex generators, *International journal of heat and mass transfer*, 36(14), 3497-3508.

Oztop, H. F., Varol, Y. and Alnak, D. E., 2009, Control of heat transfer and fluid flow using a triangular bar in heated blocks located in a channel, *International Communications in Heat and Mass Transfer*, 36(8), 878-885.

Perng, S. W. and Wu, H. W. 2008, Numerical investigation of mixed convective heat transfer for unsteady turbulent flow over heated blocks in a horizontal channel, *International Journal of Thermal Sciences*, 47(5), 620-632.

Perng, S. W., Wu, H. W. and Jue, T. C., 2012, Numerical investigation of heat transfer enhancement on a porous vortex-generator applied to a block-heated channel, *International Journal of Heat and Mass Transfer*, 55(11), 3121-3137.

Smith, R. E. and Wehofer, S., 1985, From measurement uncertainty to measurement communications, credibility, and cost control in propulsion ground test facilities. *Journal of Fluids Engineering*, 107(2), 165-172.

Sohankar, A., 2007, Heat transfer augmentation in a rectangular channel with a vee-shaped vortex generator, *International Journal of Heat and Fluid Flow*, 28(2), 306-317.

Sripattanapipat, S. and Promvonge, P., 2009, Numerical analysis of laminar heat transfer in a channel with diamond-shaped baffles, *International Communications in Heat and Mass Transfer*, 36(1), 32-38.

Teamah, M. A., El-Maghlany, W. M. and Dawood, M. M. K., 2011, Numerical simulation of laminar forced convection in horizontal pipe partially or completely filled with porous material, *International Journal of Thermal Sciences*, 50(8), 1512-1522.

Valencia, A., 1999, Heat transfer enhancement due to self-sustained oscillating transverse vortices in channels with periodically mounted rectangular bars, *International Journal of Heat and Mass Transfer*, 42(11), 2053-2062.

Wu, J. M. and Tao, W. Q., 2008, Numerical study on laminar convection heat transfer in a rectangular channel with longitudinal vortex generator. Part A: Verification of field synergy principle, *International Journal of Heat and Mass Transfer*, 51(5), 1179-1191.

Yang, S. J., 2002, A numerical investigation of heat transfer enhancement for electronic devices using an oscillating vortex generator. *Numerical Heat Transfer: Part A: Applications*, 42(3), 269-284.